Particle configurations of giant $E1$ states in the $^{14}N(\gamma, p_2)$ and $^{14}N(\gamma, p_0)$ processes*

J. E. E. Baglin
IBM Thomas J. Watson Research Center, Yorktown Heights, New York 10598

E. J. Bentz†
Niels Bohr Institute, Copenhagen, Denmark

R. W. Carr
Electron Accelerator Laboratory, Yale University, New Haven, Connecticut 06520

(Received 28 January 1974)

Angular distributions and absolute cross sections have been measured for the $^{14}N(\gamma, p_2)$ and $^{14}N(\gamma, p_0)$ reactions, at giant resonance energies. The angular distributions are shown to be consistent with a model in which exclusively $(p_{1/2})^{-1}$ $(2s\,1d)$ giant dipole states populate the ^{13}C ground state by proton decay, and predominantly $(p_{3/2})^{-1}$ $(2s\,1d)$ giant dipole states feed the $\frac{3}{2}^-$ state of ^{13}C at 3.68 MeV. Branching calculations based on established spectroscopic factors further support this model. It is inferred that the ^{14}N dipole states of $(p_{3/2})^{-1}$ $(2s\,1d)$ character, which carry $\sim 90\%$ of the $E1$ strength and which dominate the (γ, p_2) process studied, do not contribute significantly to the (γ, p_0) process which has often previously been treated as representative of $E1$ absorption.

[NUCLEAR REACTIONS $^{14}N(\gamma, p_2)$, (γ, p_0), $E_\gamma = 19$–25 MeV; measured $\sigma(E_\gamma; E_p; \theta)$. Deduced $E2$, $M1$ excitation strength. Inferred parent $E1$ configurations.]

INTRODUCTION

The photonuclear giant resonance of ^{14}N is expected to derive most of its $E1$ photon absorption strength from excitations of a single particle from a $p_{3/2}$ state to a $2s$-$1d$ state.[1,2] A minor contribution is expected in addition from promotion of $p_{1/2}$ particles to the $2s$-$1d$ shell. The $E1$ absorption is presumably accompanied by $E2$ or $M1$ absorption processes which may interfere with the $E1$ process.

When a particular giant resonance single-particle state decays by neutron or proton emission, the configuration of the residual state of ^{13}N or ^{13}C will be strongly correlated with that of the parent excited state of ^{14}N. A study of decay branching[3] in the (γ, p) process shows a selective population in residual ^{13}C of several purely $(p_{3/2})^{-1}$ states (at 3.68, 7.55, 8.86, and 11.72 MeV), and of the $(p_{1/2})^{-1}$ ground state. (In such processes, the excited nucleon is probably itself the particle which is emitted, leaving behind a simple hole configuration.[4])

The $^{14}N(\gamma, p_0)$ cross section and angular distribution have been studied experimentally in considerable detail.[5-7] However the ground-state branching accounts for only 9% of all the giant resonance decays. Further, since it probably derives mainly from ^{14}N states formed by $p_{1/2}$ particle promotion, it cannot be expected to provide direct information about the dominant giant resonance mode. Hence experimental studies of the (γ, p_2) (3.68 MeV) and higher-order processes which more closely represent the main absorption process are of particular significance at this time.

In the present experiment, we have obtained differential cross sections for the (γ, p_2) process as a function of angle and energy, between excitation energies of 19 and 25 MeV. The resulting angular distributions were used to examine the nature of the contributing parent states in the ^{14}N giant resonance, and also to estimate the extent of $E2$ or $M1$ contributions to the photon absorption at these energies.

New data were concurrently obtained for ^{14}N-(γ, p_0) angular distributions. These have been used to make direct comparisons with the (γ, p_2) observations. In the light of the observed branching and of constraints placed on possible decay channels by the observed angular distributions, we proceed finally to examine the branching predictable from known spectroscopic factors for ^{13}C states, assuming simple particle configurations in the excited states of ^{14}N.

EXPERIMENT

A thin-target bremsstrahlung beam was directed through a target of nitrogen gas, and spectra of the resulting photoprotons were observed with 2-mm deep Si(Li) detectors placed at 20, 45, 65, 90, 115, 135, and 160° to the beam axis. The equipment layout is shown in Fig. 1. Both equipment and technique were similar to those reported in

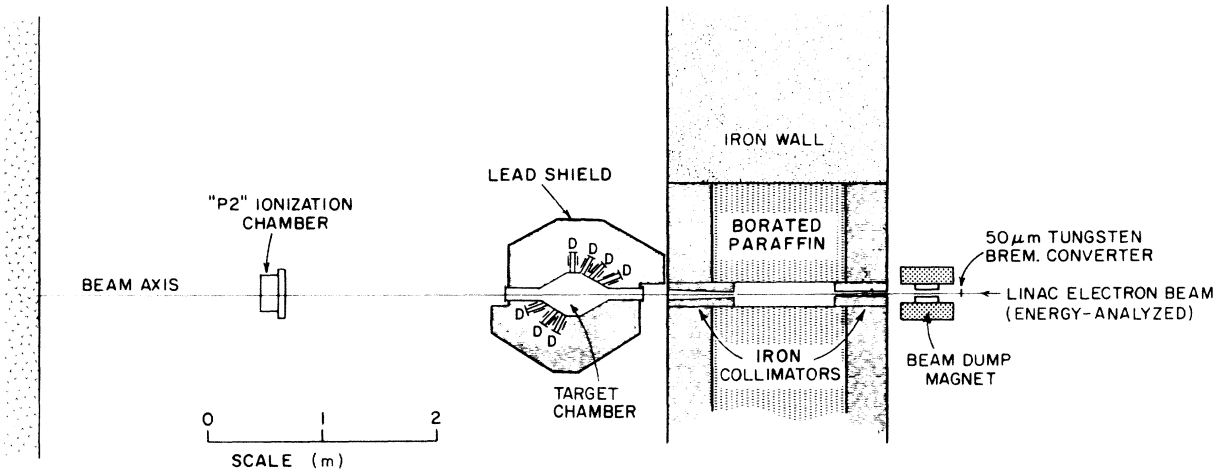

FIG. 1. Experimental layout for $^{14}N(\gamma,p_2)$, (γ,p_0) measurements. A Si(Li) proton detector attached to a cold finger was located at each of the positions marked D. The electron beam was energy-analyzed with full width at half-maximum of ~0.3%.

Refs. 5 and 8, to which reference should be made for complete details of the system.

The energy-analyzed electron beam from the 6% duty factor Los Alamos Electron Prototype Accelerator produced bremsstrahlung at a 0.005 cm tungsten converter, after which a sweeping magnet dumped the residual electrons downwards into a water-cooled tank below the beam plane. The photon beam was finely collimated by tapered iron collimators inset in the 2 m shield wall isolating the linac and electron dump from the target room.

The x-ray beam entered the target chamber through a 0.005 cm Mylar window, located so as to be shielded from the view of each of the seven cooled Si(Li) proton detectors attached to arms of the target chamber. Secondary electrons produced when the beam strikes such a window (or the target gas) are a principal potential source of large piled-up background pulses in the Si(Li) detectors. In order to further shield each detector we used a magnetic trap consisting of a permanent magnetic field of 1.2 kG covering a 15-cm long entry channel lined with baffles, in to which beam-originated electrons of energies up to 15 MeV would be deflected.

The N_2 gas filling the target chamber was maintained at a pressure of 30 Torr and its temperature and absolute pressure were recorded for each run. The effective target volume was defined by the cylindrical profile of the x-ray beam (approximately 5 cm diameter). Geometrical efficiency for each detector was determined by computation using the formulation of Silverstein,[9] and measured dimensions of the target chamber and the beam radius. Uncertainties in these determinations imply a net absolute uncertainty of ±2% in the geometrical efficiency value obtained.

After leaving the target chamber via a second thin Mylar window, the beam was intercepted by a "P2" ionization chamber[10] at the back of a "cave" of boraffin shielding intended to minimize the counter background effects due to photoneutrons produced in the chamber walls. The absolute calibration of such an instrument is expected to be good to ±3%.[10] It has a known, flat response to bremsstrahlung of end-point energies between 10 and 40 MeV. Its current was integrated using an ORTEC Model 439 integrator.

Photoproton spectra were obtained simultaneously from the seven Si(Li) detectors, their signals being multiplexed to a single analog-to-digital converter and stored on-line. Energy calibration of these spectra was referenced to peaks at 22.10 and 24.15 MeV in the $^{16}O(\gamma,p)$ spectrum—whose energies were independently derived in Ref. 11.

TREATMENT OF DATA

Dominant residual states

Figure 2 shows the schematic energy level diagram for the ^{14}N-^{13}C system, together with lines indicating the dominant reported decay branches from the ^{14}N giant resonance states.

It has been demonstrated[12,13] in studies of spectra of ^{13}C decay γ rays that the branching is weak from giant resonance states of ^{14}N to the $\frac{1}{2}^+$ and $\frac{5}{2}^+$ states of ^{13}C at 3.09 and 3.85 MeV. This is evident in the $^{14}N(\gamma, x\gamma')$ spectrum shown in Fig. 3, which was taken[12] using a 30 cm^3 Ge(Li) detector to observe a liquid nitrogen target ir-

radiated with 26 MeV bremsstrahlung. Gellie *et al.*[3] have also identified almost all of the dipole state decay strength in transitions to ^{13}C states at 0.00, 3.68, 7.55, 8.86, and 11.72 MeV (the latter three states proceeding to decay via sequential neutron emission to ^{12}C). For purposes of simplicity, we feel justified for the following discussion in ignoring other possible residual state branches of the $^{14}N^*$ decay, and assuming, in particular, that negligible branching occurs to the $\frac{1}{2}^+$ and $\frac{5}{2}^+$ states at 3.09 and 3.85 MeV.

Derivation of (γ,p_2),(γ,p_0) cross sections

The energy E_p of a photoproton emitted from a ^{14}N nucleus whose excitation energy is E_γ and leaving behind a residual ^{13}C nucleus in an excited state E_R is given approximately by

$$E_p = \tfrac{13}{14}[E_\gamma - (E_R + E_{th})], \quad (1)$$

where E_{th} is the threshold energy for the reaction to occur. Hence in a proton spectrum produced by a bremsstrahlung beam, the highest-energy protons (for an interval of 3.4 MeV) (group A) can only arise from (γ,p_0) processes. Protons from 3.4 to 7.0 MeV below the highest energy (group B) can come from (γ,p_0) or (γ,p_2) processes. Protons of still lower energy (group C) can arise in (γ,p_0) or (γ,p_2), or in processes populating the more highly excited ^{13}C states.

We obtained experimental spectra using bremsstrahlung maximum energies of 26.0, 24.0, 22.0, and 20.0 MeV. In each spectrum the ground state proton group (group A) was used to obtain directly a portion of the (γ,p_0) cross section by dividing out the weighting of the bremsstrahlung spectrum [Schiff thin target averaged-over-angles spectrum, Eq. 3BS(e), Ref. 14]. Being somewhat sensitive to our choice of analytic spectrum for bremsstrahlung, the top 0.5 MeV of each spectrum was not used. The remaining data from successive runs at different electron energies were then checked for consistency in the 1 MeV intervals of energy overlap, and an averaged $^{14}N(\gamma,p_0)$ cross section was obtained, covering the range $E_\gamma = 18$ to 26 MeV.

With the (γ,p_0) cross section established, its contribution to the "group B" portion of each proton spectrum was computed by weighting σ-(γ,p_0) with the Schiff bremsstrahlung function. This (γ,p_0) contribution was subtracted leaving a group B energy interval of each spectrum, 3.8 MeV wide, arising only from the (γ,p_2) process. By dividing out the appropriate bremsstrahlung weighting, these portions of spectra were reduced to cross sections and tested for consistency in

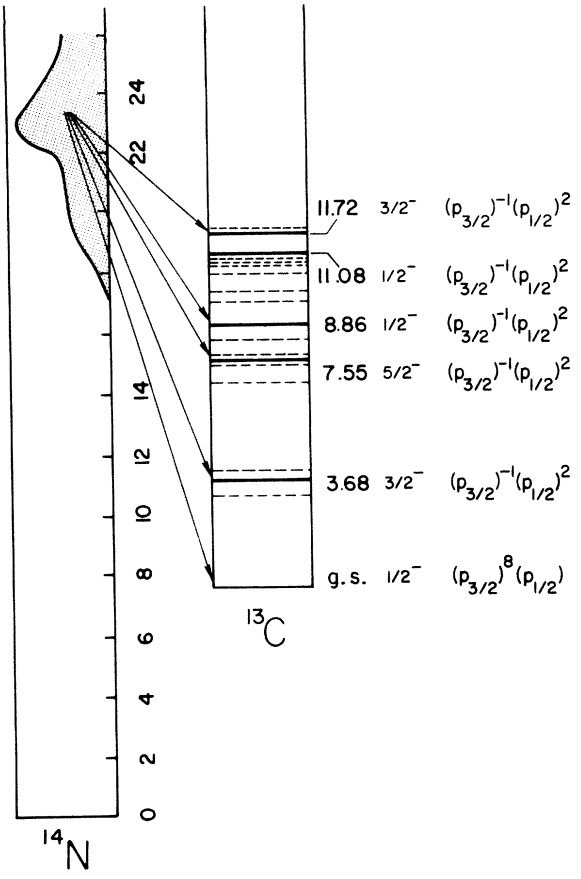

FIG. 2. $^{14}N(\gamma,p)^{13}C$ schematic level diagram. Only observed dominant decay modes of the ^{14}N giant resonance states are indicated. Configurations dominant in those residual ^{13}C states are quoted from Ref. 20. ^{13}C states not discussed here are indicated by dashed lines.

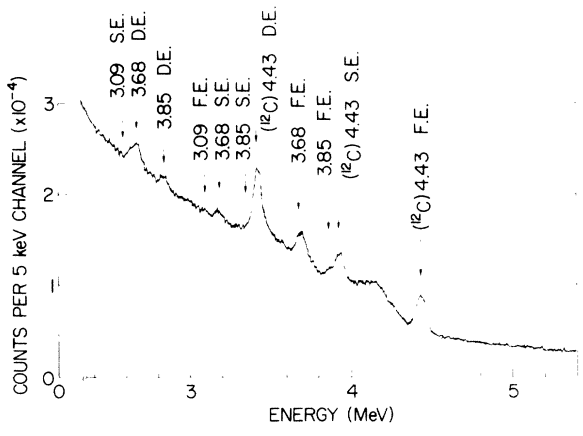

FIG. 3. $^{14}N(\gamma,x\gamma')$ spectrum taken with 26 MeV incident bremsstrahlung. Locations are indicated for full energy (FE), single escape (SE), and double escape (DE) peaks expected from all candidate decays of $^{13}C^*$ and from the 4.43 MeV state of ^{12}C formed in the (γ,np) process.

overlap regions, in the same way as we handled the (γ, p_0) data. Finally, a composite (γ, p_2) cross section curve for ^{14}N excitations of 19 to 25 MeV was derived.

Attempts to apply the same procedure again in order to derive the $(\gamma, p_{7.6\,\mathrm{MeV}})$ and higher order cross sections were not satisfactory due to lack of statistical accuracy, background effects, and possible confusion with low energy protons arising from the (γ, np) sequential decay. By contrast, in no instance in our (γ, p_2) analysis could protons from the (γ, np) process have been energetically eligible to contribute to the spectral regions used.

In all cases of overlapped cross section data taken with successive bremsstrahlung energies, our points agreed within statistics and showed no systematic disparities. This fact justifies our confidence in the validity of the Schiff spectral shape used in the analysis.

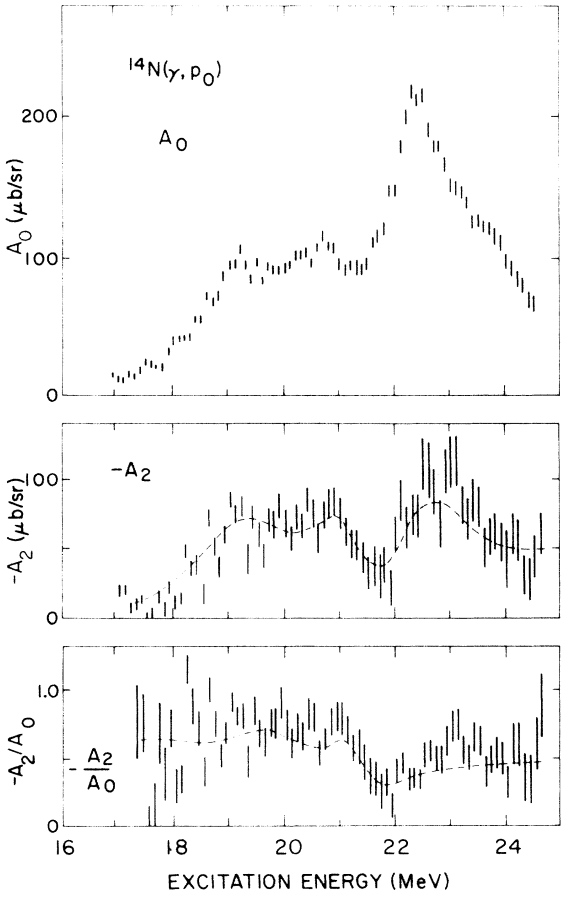

FIG. 4. ^{14}N(γ, p_0). Angular-distribution coefficients $A_0(=\sigma/4\pi)$, A_2, and the ratio A_2/A_0, plotted as functions of excitation energy in ^{14}N. Dashed lines indicate values obtained previously (Ref. 5).

Legendre coefficients

The derivation of both (γ, p_0) and (γ, p_2) differential cross sections was carried out as described for each of the angles of observation, in excitation energy bins of width 100 keV for (γ, p_0) and 200 keV for (γ, p_2). For each bin, the 7-angle angular distribution was then least-squares fitted with a Legendre polynomial series of the form

$$\frac{d\sigma}{d\Omega}(\theta) = A_0 + A_1 P_1(\cos\theta) + A_2 P_2(\cos\theta) + A_3 P_3(\cos\theta) + A_4 P_4(\cos\theta)\,. \quad (2)$$

Statistical uncertainties in the original spectra were propagated cumulatively through the processes of spectrum stripping and through the subsequent Legendre fitting.

The resulting coefficients A_0–A_4 and the ratio A_2/A_0 are plotted as functions of excitation energy for the (γ, p_0) and (γ, p_2) reactions in Figs. 4–7.

COMPARISON WITH OTHER MEASUREMENTS

Ground state cross section

The coefficient A_0 for the (γ, p_0) process is displayed in Fig. 4. These data are considered by the authors to supersede the A_0 curve derived in our earlier work, due to more certain beam ener-

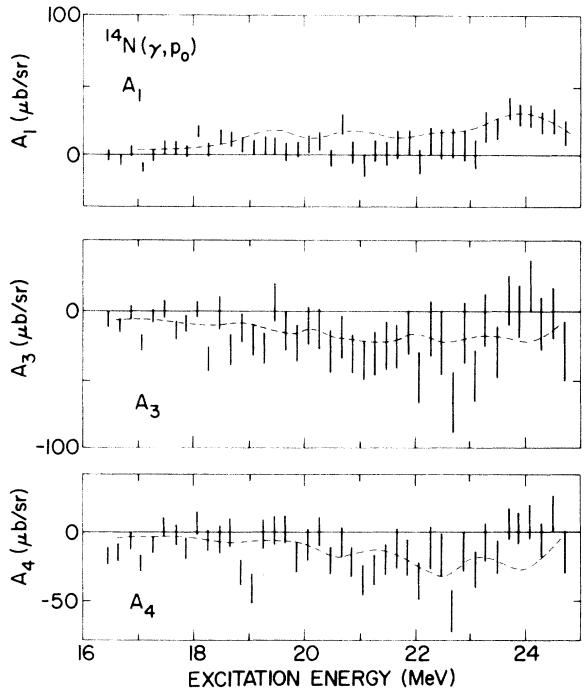

FIG. 5. ^{14}N(γ, p_0). Angular-distribution coefficients A_1, A_3, and A_4. Dashed lines indicate values obtained previously (Ref. 5).

gy control. The electron beams used in the present experiment were energy analyzed with a calibrated magnetic analyzer system, while those of Ref. 5 were not.

The values obtained for A_2, A_3, and A_4 were consistent with those of Ref. 5, as shown by the dashed curves in Fig. 4. New values of A_1 seem mostly to be smaller than those of Ref. 5, but are of similar magnitude (small).

In Fig. 8, we compare the 90° differential cross section for $^{14}N(\gamma, p_0)$ (present experiment) with that derived by detailed balance from $^{13}C(p, \gamma_0)$ data of O'Connell *et al.*[6] The two results are in good agreement. One would expect to find a similar 90° cross section for the $^{14}N(\gamma, n_0)$ reaction. This is supported in fact by the data of Ref. 3, whose general energy dependence and absolute cross section are consistent with the present results. The (γ, n_0) data of Ref. 3 appear, however, to be displaced upwards in energy by about 0.5 MeV relative to the (γ, p_0) and (p, γ_0) curves.

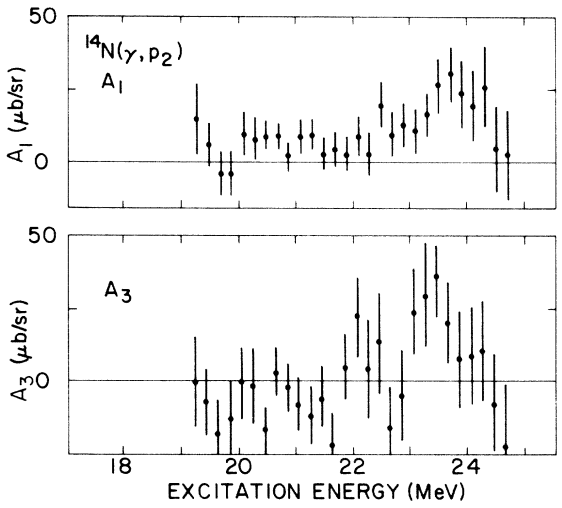

FIG. 7. $^{14}N(\gamma, p_2)$. Angular-distribution coefficients A_1 and A_3. A_4 values obtained were not statistically different from zero.

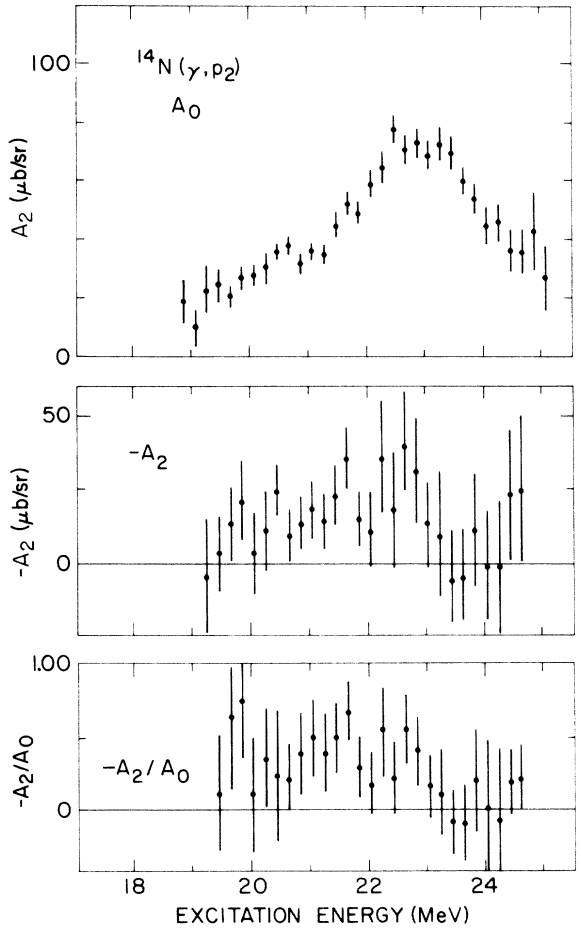

FIG. 6. $^{14}N(\gamma, p_2)$. Angular-distribution coefficients $A_0 (= \sigma/4\pi)$, A_2, and the ratio A_2/A_0, plotted as functions of excitation energy in ^{14}N.

Total absorption cross section

We now have available measured cross sections for the (γ, p_0) and (γ, p_2) reactions (this work) and the total neutron-producing cross section $[\sigma(\gamma, n) + \sigma(\gamma, np)]$ from Ref. 15. Other decay channels should make only minor contributions to the total photon absorption cross section in this energy range.[16,17] Hence we would expect the sum of these cross sections to match closely the photon absorption cross section reported by Bezic *et al.*[18]

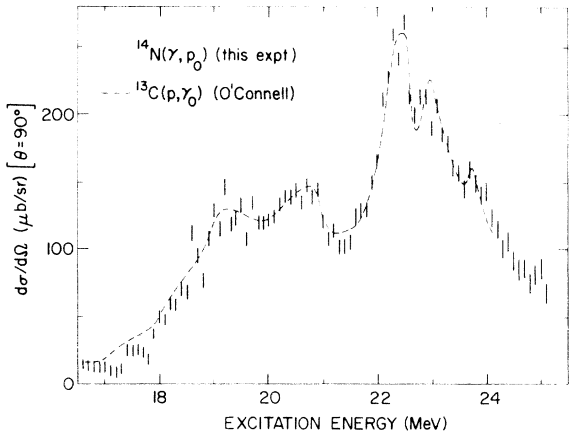

FIG. 8. Comparison of $\sigma(\gamma, p_0)$ (present work) with values derived by detailed balance from the $^{13}C(p, \gamma_0)$ data of Ref. 6.

In Fig. 9 such a comparison is made. The energy dependences of the sum curve and the measured absorption curve are very similar. However, it should be pointed out that in order to obtain such correspondence, the (γ, n) data needed to be arbitrarily shifted down in energy by 0.5 MeV. The amended energy scale seems to be supported by the older (γ, n) work of Ref. 19, whose scale agrees with the present data and Ref. 18. Of greater concern is the factor of 0.7 between Bezic's absorption curve and the present component sum. The factor applied to Bezic's data would produce a value for the integral cross section up to 30 MeV representing about 70% of the classical dipole sum—similar to his observations for ^{12}C and ^{16}O. The reduction thus produces pleasing systematics, although its justification is not clear. A new absolute absorption measurement would be very desirable in order to resolve this question.

DISCUSSION

Owing to the large number of possible channels for the (γ, p_0) and (γ, p_2) processes and the variety of excitation mechanisms possible in ^{14}N, a unique description of the (γ, p) processes cannot be constructed on the basis of presently available experimental data. In the discussion which follows, we have generally attempted to identify the simplest dominant mechanisms which can satisfactorily account for the present new results together with other current data.

Branching

The significant differences in cross section shape for the (γ, p_0) and (γ, p_2) processes are

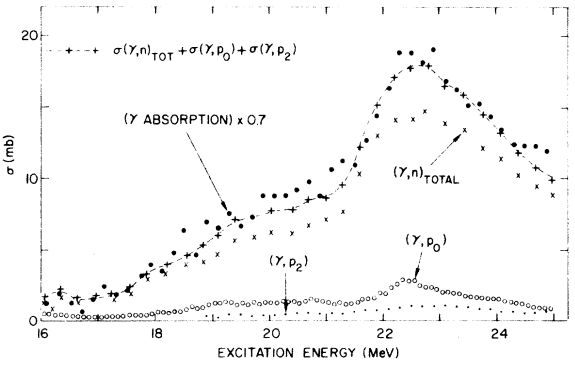

FIG. 9. Total photon absorption cross section in ^{14}N. Displayed are the partial cross sections $\sigma(\gamma,p_0)$ and $\sigma(\gamma,p_2)$ (present work) and $[\sigma(\gamma,n)+\sigma(\gamma,np)+\sigma(\gamma,pn)]$ (Ref. 15, energy scale lowered by 0.5 MeV). Their sum is compared with observed absorption data (Ref. 18, multiplied by 0.70).

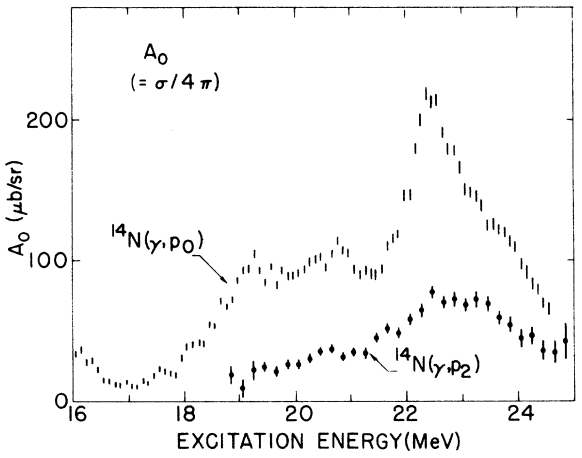

FIG. 10. Comparison of the energy dependence of cross sections for $^{14}N(\gamma,p_0)$ and $^{14}N(\gamma,p_2)$.

emphasized in Fig. 10. It is instructive to plot the branching ratio for decays from the giant resonance states to each of the ground and 3.68 MeV states as shown in Fig. 11, using the total absorption cross section reported by Bezic *et al.*[18] as a reference. It is evident from these curves that the shape of the (γ, p_2) cross section follows closely that of the total absorption giant resonance.

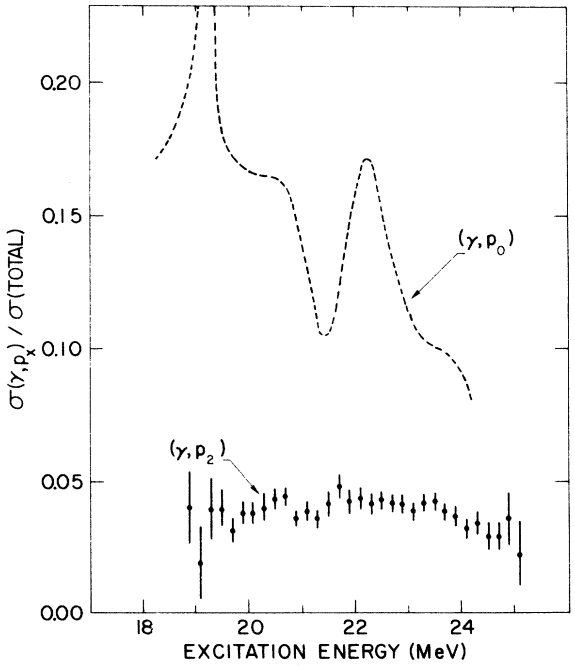

FIG. 11. Branching to ^{13}C ground state. Energy dependence of the ratio of $\sigma(\gamma,p_0)$ and $\sigma(\gamma,p_2)$ to σ (total absorption) of Ref. 18.

This implies that those ^{14}N states which dominate the giant resonance absorption are the parent states of the ^{13}C(3.68 MeV)+p system. In contrast, the (γ, p_0) cross section does not have the same energy dependence as that of photon absorption, implying that it originates in a different set of parent states of ^{14}N which are not dominant in the absorption process.

As mentioned above, the ^{13}C ground state has exclusively $(p_{1/2})^{-1}$ character. Hence the above observation confirms our expectation that it will be populated mainly via $(p_{1/2})^{-1}$ $(2s1d)$ states in ^{14}N—states expected to occupy only a few percent of the total $E1$ strength.[1]

The 3.68 MeV state of ^{13}C has mixed character, dominated by a $(p_{3/2})^{-1}$ configuration with a pair of $(p_{1/2})$ particles having $T=0$ or $T=1$.[15] We expect the $E1$ strength to lie mainly in $p_{3/2}$ particle excitation. Hence, it is not surprising to find that the (γ, p_2) cross section reflects the energy dependence of the total absorption curve, which is presumably simply that of the cross section for exciting the $(p_{3/2})^{-1}$ $(2s1d)$ states in ^{14}N.

We therefore infer that the ^{14}N(γ, p_0) cross section reflects the giant $E1$ resonance for $(p_{1/2})^{-1}$ $(2s1d)$ states, while the ^{14}N(γ, p_2) cross section reflects the behavior of the $E1$ resonance for $(p_{3/2})^{-1}$ $(2s1d)$ states. We also note from the configurations of ^{13}C states shown in Fig. 2 that no other $(p_{1/2})^{-1}$ states besides the ^{13}C ground state have been seen to receive significant branching in the (γ, p) process. Hence we conclude that the ^{14}N(γ, p_0) cross section probably constitutes almost *all* of the ^{14}N(γ, p) giant resonance which is excited by $(p_{1/2})$ particle promotion.

We thus have a measure of the fraction of (γ, p) giant resonance excitation which occurs by $p_{1/2}$ particle promotion, as a function of energy. Its integral cross section from 18 to 25 MeV is (9 ± 1) MeV mb, or 9% of the integral absorption cross section to 25 MeV.[18] Since the ^{14}N(γ, n_0) cross section has been observed[3] to be almost identical to that for (γ, p_0), we may conclude that the $(p_{1/2})$ promotion resonance strength is about 18% of the total giant resonance.

This leads to two further observations: (i) Exhaustive studies of the ^{14}N(γ, p_0) cross section (such as have been pursued in the past) are not likely to give much information about the dominant giant resonance modes of ^{14}N. (ii) Further examination of the (γ, p_2) process *is* likely to yield direct evidence of the $(p_{3/2})$-promotion resonances which carry about 80% of the $E1$ strength.[21]

Considering the significance of these conclusions if substantiated, we proceed to examine our angular distribution data for consistency with the proposed allotment of $p_{1/2}$ and $p_{3/2}$ excitations. We then check the implied model of single-particle migration with a simple decay branching-ratio calculation.

Angular Distributions

E1/M1, E1/E2 interference. In both (γ, p_0) and (γ, p_2) processes the coefficients A_1, A_3, and A_4 are small, as indicated in Figs. 5 and 7. In the (γ, p_2) study, our fitted A_4 values were not statistically different from zero, and hence they are not plotted here. The coefficient A_1 consists entirely of $E1/M1$ and $E1/E2$ interference terms; A_3 consists only of $E1/E2$ terms. In the (γ, p_0) case, A_1 and A_3 display somewhat similar energy dependence. However, they show no obvious correlation with structures in the A_0 envelope. Since the A_0 curve is almost pure $E1$ in character, a possible inference is that the same few $E2$ states cause interference in both coefficients. Some similarity is also evident in the A_1 and A_3 data for the (γ, p_2) reaction. In both processes, the interfering amplitude needed to produce observed values of A_1 and A_3 would be of the order of 8% of the $E1$ amplitude at a given energy. The contribution of these $E2$ components to the total absorption cross section is thus of the order of 1%—which can be neglected when we discuss the major $E1$ transitions.

E1 channels. In considering the $E1$ channels, we discuss only the coefficients A_0 and A_2 and neglect terms involving $M1$ and $E2$ contributions. The ^{14}N ground state has $J^\pi = 1^+$ and hence an $E1$ excitation can lead to a state of $J^\pi = 0^-$, 1^-, or 2^-. The number of possible decay channels leading to a given residual state of ^{13}C is too large to allow us to solve for each phase and amplitude using available data. However, some conclusions can be drawn about dominant channels.

In the notation of Carr and Baglin,[22] we define $(E1, ljs)$ as the matrix element associated with an electric dipole excitation of ^{14}N to a state of spin j which decays by emitting a proton of orbital angular momentum l, with channel spin s describing the decay channel.

We then write for $E1$ transitions

$$(24/\lambda_\gamma^2)\frac{d\sigma}{d\Omega}(\theta) = \alpha_0 + \alpha_2 P_2(\cos\theta), \tag{3}$$

where

$$\alpha_\nu = \sum_{u v} C_{t_u t_v \nu} \operatorname{Re}\{(E1, ljs)_u^* (E1, ljs)_v\},$$

with t_u and t_v referring to all parameters of channels u and v.

The possible $E1$ reaction channels together with

their coefficients C are listed in Table I for the (γ, p_0) process and in Table II for the (γ, p_2) process.[22]

(γ, p_0) data. We note from Fig. 4 that in the (γ, p_0) process, $A_2/A_0 (= \alpha_2/\alpha_0)$ has a value between -0.7 and -0.9 at energies below 21 MeV, and it stabilizes again at about -0.5 above 22.5 MeV. As discussed in Ref. 5, the high energy value could readily be satisfied by assuming a predominant (220) channel ($A_2/A_0 = -0.5$). However, in order to generate the observed large value of $A_2/A_0 = -0.7$, using the coefficients of Table I, a very selective set of phases and interfering channel amplitudes is needed. At the least, interference of (000) and (220) channels with favorable phases is required.

It is gratifying to observe that these channels do represent the two direct processes in which a $p_{1/2}$ particle is promoted to the s-d shell and then emitted, leaving the $(p_{1/2})^{-1}$ ground state of ^{13}C. The intermediate resonant states in this case would be characterized by

$$(000): (p_{1/2})^{-1} s_{1/2}, \quad j = 0;$$

$$(220): (p_{1/2})^{-1} d_{3/2}, \quad j = 2.$$

Our data are thus consistent with the dominance of these channels in the (γ, p_0) process. The picture including mainly the (220) channel above 22.5 MeV and a mixture of this with (000) below 21 MeV is consistent with the energy distribution of $j = 0$, 1, and 2 strengths implied by the single-particle model calculation of Cooper.[23]

(γ, p_2) data. The energy dependence of A_2/A_0 in the (γ, p_2) process is less clearly defined than that of the ground state channel, as seen in Fig. 6. For energies below 23 MeV, a single value $(A_2/A_0) = -0.4$ would satisfy the data; at higher energies, (A_2/A_0) seems to approach zero. In this case, many combinations of possible channel amplitudes and phases can be found which fit these values of (A_2/A_0). However, it is interesting to note that the (A_2/A_0) values can be reproduced by invoking only channels in which a $p_{3/2}$ particle is promoted to the s-d shell before escaping to leave the residual ^{13}C(3.68 MeV) configuration. Candidate channels and corresponding ^{14}N states are:

$$\left.\begin{array}{ll} (212): (p_{3/2})^{-1} d_{3/2}, & j = 1 \\ (022): (p_{3/2})^{-1} s_{1/2}, & j = 2 \end{array}\right\} \rightarrow A_2/A_0 \gtrsim -0.4,$$

$$\left.\begin{array}{ll} (202): (p_{3/2})^{-1} d_{3/2}, & j = 0 \\ (222): (p_{3/2})^{-1} d_{3/2}, & j = 2 \\ (212): (p_{3/2})^{-1} d_{5/2}, & j = 1 \\ (222): (p_{3/2})^{-1} d_{5/2}, & j = 2 \\ (011): (p_{3/2})^{-1} s_{1/2}, & j = 1 \end{array}\right\} \text{ any or all} \rightarrow A_2/A_0 \sim 0.$$

As in the case of the (γ, p_0) analysis, these conclusions result simply from empirical trial and error efforts to fit the observed coefficients with groups of one, two, or three reaction channels. While these assignments are admittedly speculative, they serve to illustrate that the (γ, p_2) data readily fit the proposed pure $p_{3/2}$ excitation model.

SPECTROSCOPIC FACTORS

First-order estimates of the decay branching of ^{14}N dipole states can be made on the basis of well-known spectroscopic factors for the ^{13}C + p sys-

TABLE I. Angular-distribution coefficients describing the $E1$ components of the ^{14}N(γ, p_0) reaction. The notation used is that of Eq. (2) of Ref. 17, from which this table is derived.

$(ljs)_u$	$(ljs)_v$	C_0	C_2
000	000	1.00	···
000	220	···	3.16
011	011	3.00	···
011	211	···	−2.12
011	221	···	−4.74
211	211	3.00	0.75
211	221	···	−3.35
220	220	5.00	−2.50
221	221	5.00	−1.25

TABLE II. Angular-distribution coefficients describing the $E1$ components of the ^{14}N(γ, p_2) reaction. The notation used is that of Eq. (2) of Ref. 17, from which this table is derived.

$(ljs)_u$	$(ljs)_v$	C_0	C_2
202	202	1.00	···
202	022	···	1.41
202	222	···	−1.69
202	422	···	2.27
011	011	3.00	···
011	211	···	−2.12
011	221	···	−4.74
211	211	3.00	0.75
211	221	···	−3.35
212	212	3.00	−0.75
212	022	···	3.67
212	222	···	−2.20
212	422	···	−3.93
221	221	5.00	−1.25
022	022	5.00	···
022	222	···	4.18
222	222	5.00	0.54
222	422	···	1.92
422	422	5.00	−1.79

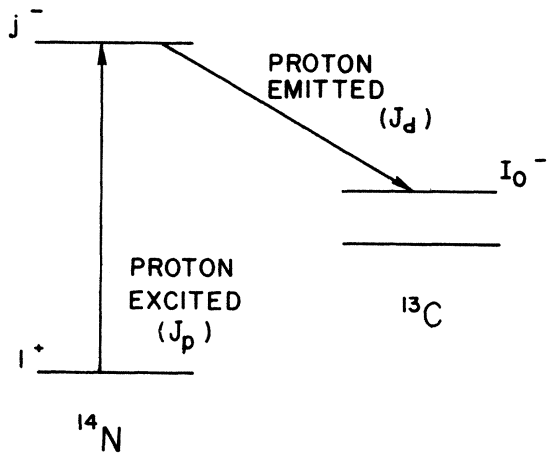

FIG. 12. Schematic for photoparticle emission showing angular momenta involved.

TABLE III. Branching in the proton decay of specific electric dipole states of ^{14}N to some dominant residual states of ^{13}C, as calculated using Cohen-Kurath spectroscopic factors. For each ^{14}N state, its fractional branching among residual states is quoted. No account is taken of barrier penetrabilities, which will in practice modify the effect of these quantities.

		^{13}C residual state energy in MeV (I^{π}_0)					
^{14}N $E1$ state Configuration	j	0.00 ($\frac{1}{2}^-$)	3.68 ($\frac{3}{2}^-$)	7.55 ($\frac{5}{2}^-$)	8.86 ($\frac{1}{2}^-$)	11.08 ($\frac{1}{2}^-$)	11.72 ($\frac{3}{2}^-$)
$(p_{1/2})^{-1}(2s1d)$	2	0.66	0.06	···	0.05	0.19	0.01
$(p_{1/2})^{-1}(2s1d)$	1	0.72	0.01	···	0.06	0.21	···
$(p_{1/2})^{-1}(2s1d)$	0	0.72	0.01	···	0.06	0.20	···
$(p_{3/2})^{-1}(2s1d)$	2	···	0.02	0.70	0.07	···	0.20
$(p_{3/2})^{-1}(2s1d)$	1	···	0.06	0.24	0.19	···	0.49
$(p_{3/2})^{-1}(2s1d)$	0	···	0.03	0.18	0.52	···	0.24

tem.[24,25] For notation, we refer to Fig. 12, in which angular momenta describing a single reaction channel are indicated.

Amplitude $A(J_p^-, J_d)$ is defined for the channel shown, in which a proton initially having angular momentum J_p is excited by the incoming photon, producing a ^{14}N state of spin j. This state then decays by ejecting the proton whose angular momentum is J_d in the excited ^{14}N nucleus. The residual ^{13}C configuration has spin I_0.

We may write[26]

$$A^2(J_p^-, J_d) \sim (2J_d+1)^{-1}[(I_0 J_d M_0 J_z - M_0 | j J_z) W(I_0 J_p j1; 1J_d)\langle \underline{a}^{J_d} | \underline{b}^{J_d\dagger}\rangle \langle \text{g.s.}^{14}\text{N} || \underline{a}^{J_p\dagger} || I_0{}^{13}\text{C}\rangle]^2 . \quad (4)$$

Summing over z components, we obtain

$$A^2(J_p^-, J_d) \sim P(J_d) S(J_p I_0)[(2j+1)/(2J_d+1)] W^2(I_0 J_p j1; 1J_d) , \quad (5)$$

where S is the spectroscopic factor for ^{13}C + p and $P(J_d)$ is a penetrability factor for the escaping proton. Equation (5) thus displays the dominant terms which will influence decay branching from the excited ^{14}N state. We here consider only $E1$ excitation channels. Further, since photoproton energies in the ^{14}N case are large ($\gtrsim 8$ MeV), and we are dealing only with s- or d-wave protons, we have assumed a penetrability P equal to unity.

In order to estimate qualitatively the branching patterns expected, we have evaluated the product in Eq. (5), using Cohen-Kurath spectroscopic factors,[24] and considering those negative parity single-hole residual states of ^{13}C which are accessible from $E1$ giant resonance states. The results are summarized in Table III, where the calculated branching is shown for each dipole state j, formed by promotion of either a $p_{1/2}$ or a $p_{3/2}$ particle. In the interest of simplicity, we have summed over the possible J_d values in each case. Several features of the table merit comment:

(i) Energies of the Cohen-Kurath states have been identified with experimentally understood states of ^{13}C in accord with the conclusions of Fleming *et al.*[27] In particular the $\frac{1}{2}^-$ state at 11.08 MeV is identified as the third $\frac{1}{2}^-$ state of Ref. 24, and the $\frac{3}{2}^-$ state at 11.72 MeV is taken to be the second $\frac{3}{2}^-$ state of the Cohen-Kurath tabulation. The $\frac{3}{2}^-$ state of ^{13}C at 9.9 MeV is not considered to have a simple $(p)^{-1}$ structure,[27] and it was not included in the computation. There is in fact no experimental certainty that any decay to this state occurs at all.[3] For similar reasons, the $\frac{7}{2}^-$ state at 10.75 MeV has also been omitted from the present discussion.

(ii) The approximations and model assumptions are crude and the table is intended to indicate trends rather than precise branching values

(iii) Less than 1% branching to the ground residual state is indicated from a $(p_{3/2})^{-1}$ $(2s1d)$ dipole state. In other words, the ground-state reaction is predicted to occur exclusively via $(p_{1/2})^{-1}$ $(2s1d)$ states. This is in fact consistent with our channel assignments based on experi-

mental (γ, p_0) angular distributions, which involve only $(p_{1/2})^{-1}$ $(2s1d)$ states.

(iv) At least 70% of the proton decays of $(p_{1/2})^{-1}$ $(2s1d)$ states populate the ^{13}C ground state directly. (In fact, due to barrier effects, an even stronger branching to the ground state will occur). The observed ground state cross section can thus be expected to represent most of the cross section for $p_{1/2}$ proton excitation in the $E1$ resonance of ^{14}N.

(v) The ^{14}N(γ, p_2) cross section will contain contributions from both $p_{1/2}$ and $p_{3/2}$ excitations. According to the calculations of Cooper[23] approximately 86% of the $E1$ strength below 26 MeV originates in excitation of $j=2$ states in ^{14}N. Hence from Table III we may estimate that the $(p_{1/2})^{-1}$ contribution to $\sigma(\gamma, p_2)$ is given by

$$\sigma(\gamma, p_2)[p_{1/2}]/\sigma(\gamma, p_0)[p_{1/2}] \approx \sigma(\gamma, p_2)[p_{1/2}, j=2]/\sigma(\gamma, p_0)[p_{1/2}, j=2] \approx 0.09 .$$

Since $\sigma(\gamma, p_0)[p_{1/2}]$ has been identified with the entire $\sigma(\gamma, p_0)$, we may write $\sigma(\gamma, p_2)[p_{1/2}]$ $\approx 0.09\,\sigma(\gamma, p_0)$. From the data of Fig. 10 we note that $\sigma(\gamma, p_2)[p_{1/2}]$ will thus constitute less than 20% of $\sigma(\gamma, p_2)$ observed. Hence we conclude that $\sigma(\gamma, p_2)$ is predominantly related to $(p_{3/2})^{-1}$ processes. This is consistent also with our ability to fit (γ, p_2) angular distributions by invoking only $(p_{3/2})^{-1}$ channels.

Hence it is suggested that the cross section envelopes shown in Fig. 10 reflect the principal energy-dependent features of the "$(p_{1/2})^{-1}$" and "$(p_{3/2})^{-1}$" processes, respectively.

(vi) The integral cross sections observed in this work, from 19 to 25 MeV, were (9 ± 1) MeV mb for ^{14}N(γ, p_0), and (4 ± 0.5) MeV mb for ^{14}N(γ, p_2). These are consistent with the branching deduced by Gellie *et al.*,[3] based on observations of (γ, n) and (γ, pn) processes.

(vii) The observations are consistent with the branching calculations by Kissener *et al.*[25] recently published. Their work is likewise based upon spectroscopic factors derived from Cohen-Kurath wave functions, and their transition strength calculations are based on a shell model with intermediate coupling. It should be pointed out, however, that our original experimental ^{14}N(γ, p_2) cross section as quoted by Kissener involved an error in data reduction. The error was located and corrected some time ago, leading to the results contained in this paper. Fortunately, the (γ, p_2) cross section of Ref. 25 now seems to agree in both magnitude and energy dependence with our experimental results.

CONCLUSION

Our measurements of giant resonance cross sections for the ^{14}N(γ, p_2) and ^{14}N(γ, p_0) processes, together with their angular distributions, have led to the tentative identification of the (γ, p_0) process with pure $p_{1/2}$-particle promotion, and to the derivation from the (γ, p_2) cross section of a component which appears to represent the alternative $p_{3/2}$-particle excitation resonance envelope. Such an experimental separation of the $E1$ resonance configurations has not previously been achieved directly. It is of particular diagnostic significance in assessing the correctness of single particle models proposed[1,4,25] to describe the giant resonance excitation of ^{14}N.

ACKNOWLEDGMENTS

We wish to record our appreciation of the generous hospitality and encouragement of Dr. Louis Rosen, Dr. E. A. Knapp, J. Busick, and the staff of the Los Alamos Electron Prototype Accelerator.

---

*Work supported in part by the U. S. Atomic Energy Commission at Yale University, New Haven, Connecticut, and at the Ames Laboratory, Iowa State University, Iowa.

†Present address: RCA David Sarnoff Research Center, Princeton, New Jersey 08540.

[1]B. S. Cooper and J. M. Eisenberg, Nucl. Phys. A114, 184 (1968).

[2]H. U. Jäger, H. R. Kissener, and R. A. Eramzhian, Nucl. Phys. A171, 584 (1971).

[3]R. W. Gellie, K. H. Lokan, N. K. Sherman, and J. I. Lodge, Can. J. Phys. 50, 1689 (1972).

[4]B. M. Spicer, Aust. J. Phys. 26, 269 (1973).

[5]R. W. Carr, J. E. E. Baglin, and E. J. Bentz, Phys. Rev. C 6, 2032 (1972).

[6]W. J. O'Connell, Ph.D thesis, Stanford University, 1970 (unpublished); and F. Riess, W. J. O'Connell, and P. Paul, Nucl. Phys. A175, 462 (1971).

[7]J. M. Dixon, Ph.D. thesis, University of Melbourne, 1972 (unpublished).

[8]J. E. E. Baglin, R. W. Carr, E. J. Bentz, and C. -P. Wu, Nucl. Phys. A201, 593 (1973).

[9]E. A. Silverstein, Nucl. Instrum. Methods 4, 53 (1959).

[10]J. S. Pruitt and S. R. Domen, National Bureau of Standards Monograph No. 48 (1962); also J. E. E. Baglin, E. J. Bentz, R. W. Carr, C. -P. Wu, and H. L. Schultz, Nucl. Instrum. Methods 104, 575 (1972).

[11]C. -P. Wu, Ph.D. thesis, Yale University, 1969 (unpublished).

[12]J. E. E. Baglin, Bull. Am. Phys. Soc. 17, 550 (1972).

This work was done in collaboration with D. McConnell, B. Thomas (Univ. of Toronto), R. Morrison and B. Cook (Iowa State Univ.), and E. J. Bentz, R. W. Carr, and C. -P. Wu (Yale Univ.)

[13]M. N. Thompson, R. J. J. Stewart, and J. E. M. Thomson, Phys. Lett. 31B, 211 (1970).

[14]H. W. Koch and J. W. Motz, Rev. Mod. Phys. 31, 920 (1959).

[15]B. L. Berman, S. C. Fultz, J. T. Caldwell, M. A. Kelly, and S. S. Dietrich, Phys. Rev. C 2, 2318 (1970).

[16]M. E. Toms, Nucl. Phys. 54, 625 (1964).

[17]J. L. Black, W. J. Caelli, W. F. Davidson, and R. B. Watson, Nucl. Phys. A153, 233 (1970).

[18]N. Bezic, D. Brajnik, D. Jamnik, and G. Kernel, Nucl. Phys. A128, 426 (1969).

[19]R. W. Fast, P. A. Flournoy, R. S. Tickle, and W. D. Whitehead, Phys. Rev. 120, 1424 (1960).

[20]G. Ball and J. Cerny, Phys. Rev. 177, 1466 (1969).

[21]It seems likely at this point that similar arguments will also apply to the case of ^{16}O.

[22]R. W. Carr and J. E. E. Baglin, Nucl. Data A10, 143 (1971).

[23]B. S. Cooper, Ph.D. thesis, University of Virginia, 1967 (unpublished).

[24]S. Cohen and D. Kurath, Nucl. Phys. A101, 1 (1967).

[25]H. R. Kissener, R. A. Eramzhian, and H. U. Jäger, Nucl. Phys. A207, 78 (1973).

[26]D. Kurath, private communication.

[27]D. G. Fleming, J. Cerny, C. C. Maples, and N. K. Glendenning, Phys. Rev. 166, 1012 (1968).

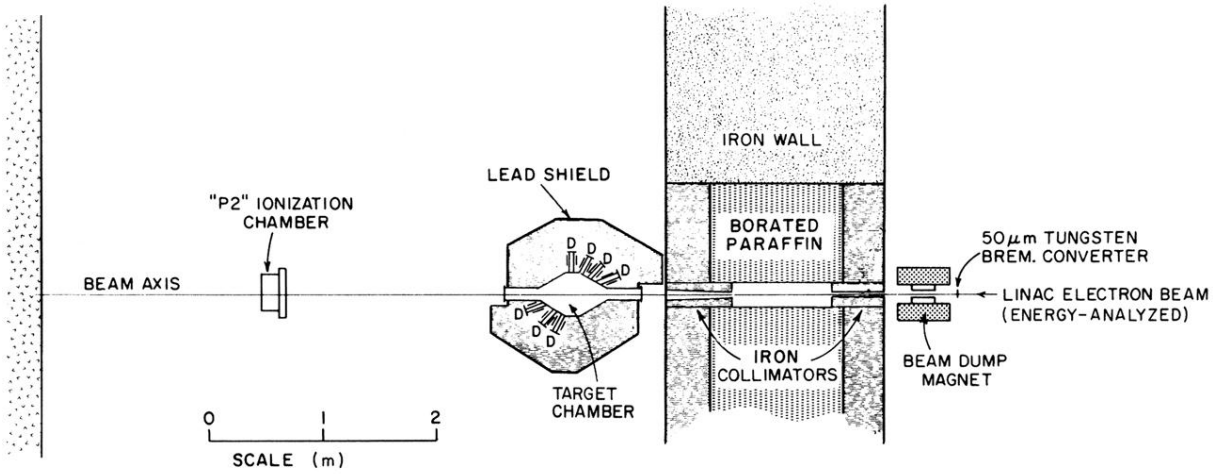

FIG. 1. Experimental layout for $^{14}N(\gamma,p_2),(\gamma,p_0)$ measurements. A Si(Li) proton detector attached to a cold finger was located at each of the positions marked D. The electron beam was energy-analyzed with full width at half-maximum of ~0.3%.

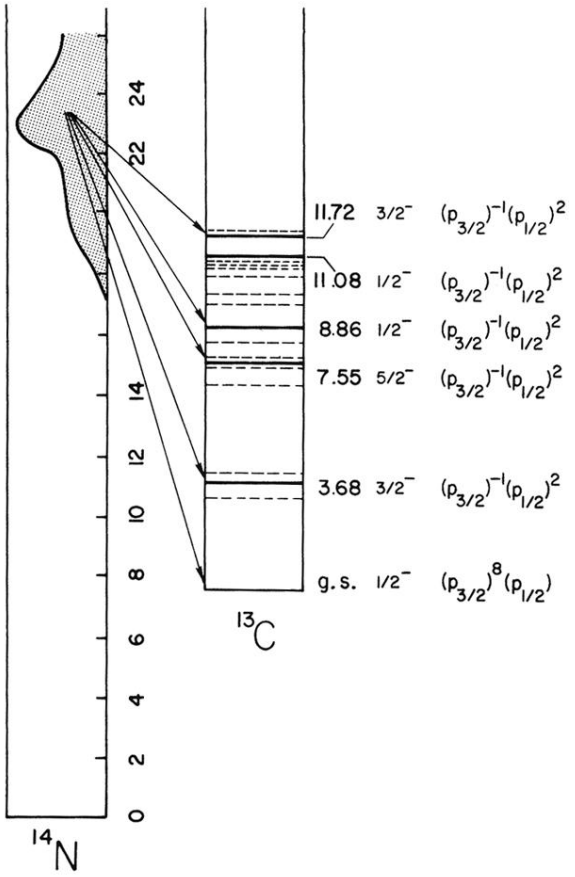

FIG. 2. $^{14}N(\gamma,p)^{13}C$ schematic level diagram. Only observed dominant decay modes of the ^{14}N giant resonance states are indicated. Configurations dominant in those residual ^{13}C states are quoted from Ref. 20. ^{13}C states not discussed here are indicated by dashed lines.